Pergamon

Int. Comm. Heat Mass Transfer, Vol. 23, No. 6, pp. 875–887, 1996
Copyright © 1996 Elsevier Science Ltd
Printed in the USA. All rights reserved
0735-1933/96 $12.00 + .00

PII S0735-1933(96)00070-X

NON-DARCY HYDROMAGNETIC FREE CONVECTION FROM A CONE AND A WEDGE IN POROUS MEDIA

Ali J. Chamkha
Department of Mechanical and Industrial Engineering
Kuwait University
P. O. Box 5969
Safat, 13060 - Kuwait

(Communicated by J.P. Hartnett and W.J. Minkowycz)

ABSTRACT

Continuum equations governing non-Darcy hydromagnetic free convection flow of an electrically conducting and heat-generating fluid over a vertical cone and a wedge adjacent to a porous medium are developed. These equations account for such effects as buoyancy, boundary and inertia effects of porous media, Hartmann effects of magnetohydrodynamics, and heat generation or absorption of fluid. Similarity variables were employed for the case of variable surface temperature and the resulting ordinary differential equations are solved numerically by an implicit, iterative, finite-difference method. Flow and heat transfer numerical results are obtained for various combinations of physical parameters. Graphical results illustrating interesting features of the physics of the problem are presented and discussed.

Introduction

The study and analysis of heat and mass transfer in porous media have been the subject of many investigations due to their frequent occurrence in industrial and technological applications. Examples of some applications include geothermal reservoirs, drying of porous solids, thermal insulation, enhanced oil recovery, packed-bed catalytic reactors, and many others. There has been considerable work done on magnetohydrodynamic free convection flow over a vertical semi-infinite plate which is based on the laminar boundary-layer approach. See, for instance, Sparrow and Cess [1], Riley [2], Kuiken [3], Takhar [4], Wilks [5,6], and Takhar and Soundalgekar [7]. The problem of convection heat transfer from a cone or a wedge has been considered previously by Vajravelu and Rollins [8], Merk and Prins [9], Hering and Gosh [10], Sparrow and Guinle

[11], Nakayama et al. [12], Gorla and Stratman [13], Watanabe and Pop [14], and Vajravelu and Nayfeh [15]. Most early studies on convection heat transfer in porous media have used Darcy's law which neglects boundary and inertia effects which are important in the presence of a solid boundary and when the flow velocity is high (i.e. the Reynold's number based on the mean pore size is greater than unity). Vafai and Tien [16] and Hong et al. [17] summarize the importance of both boundary and inertia effects in porous media.

In problems dealing with chemical reactions and dissociating fluid, heat generation in moving fluids becomes important (see, Vajravelu and Nayfeh [15]). Moalem [18] has studied the effect of temperature-dependent heat sources occurring in electrical heating on the steady-state heat transfer in a porous medium. Other works taking into account heat generation effects can be found by the early papers by Sparrow and Cess [1], Topper [19], and Foraboschi and Federico [20].

Motivated by the works mentioned above, the steady, laminar, free convection flow along a vertical cone and a wedge immersed in an electrically conducting fluid-saturated porous medium in the presence of a transverse magnetic field is considered. The surface temperature of the cone and the wedge is assumed to be variable and internal heat generation is assumed to exist. The applied magnetic field is assumed to be uniform and the magnetic Reynold's number is assumed to be small so that the induced magnetic field can be neglected. In addition, it is assumed that the external electric field is zero and the electric field due to polarization of charges is negligible.

Mathematical Formulation

Consider steady, laminar, free convection boundary-layer flow of an electrically conducting fluid over a vertical cone and a wedge adjacent to a fluid-saturated porous medium. A uniform transverse magnetic field normal to the cone and the wedge surfaces is applied. The porous medium is assumed to be of uniform porosity and permeability while the wall temperature of the cone and the wedge is assumed to be variable. The coordinate system is such that x measures the distance along the surface of the body from the apex, $x = 0$ being the leading edge, and y measures the distance normally outward. The physical model under consideration and the coordinates chosen are depicted in Fig. 1. Neglecting viscous and magnetic dissipations, and taking into account Boussinesq approximation, the boundary-layer form of the governing equations can be written as

$$\frac{\partial}{\partial x}(r^n u) + \frac{\partial}{\partial y}(r^n \mathrm{v}) = 0 \tag{1}$$

$$u\frac{\partial u}{\partial x}+\nu\frac{\partial u}{\partial y}=\nu\frac{\partial^2 u}{\partial y^2}-\frac{\sigma_0 B_0{}^2 u}{\rho}-\frac{\nu}{K}u-Cu^2+g\beta(T-T_\infty)\cos\alpha \tag{2}$$

$$\rho c(u\frac{\partial T}{\partial x}+\nu\frac{\partial T}{\partial y})=k_e\frac{\partial^2 T}{\partial y^2}+Q(T-T_\infty) \tag{3}$$

where $n=0$ corresponds to flow over a vertical wedge and $n=$ corresponds to flow over a vertical cone. x, y, and r are the tangential, normal, and radial distances as shown in Fig. 1. α is the cone or wedge half angle. u, ν, and T are the fluid x-component of velocity, y-component of velocity, and temperature, respectively. ρ, ν, c and k_e are the fluid density, kinematic viscosity, specific heat, and effective thermal conductivity, respectively. $\sigma_0, B_0, g,$ and β are the fluid electrical conductivity, the magnetic induction, the gravitational acceleration, and the volumetric thermal expansion coefficient, respectively. K and C are the respective permeability and the inertia coefficient of the porous medium. Q and T_∞ are the volumetric heat generation and ambient fluid temperature, respectively.

It should be noted that in the momemtum equation, Eq. (2), the first term on the right hand side is the boundary effect which represents the wall frictional resistance to flow along the solid boundary of the cone and the wedge. The third term on the right side is the porous medium Darcian force representing the pressure loss due to the presence of a porous medium. The fourth term on the same side is the inertia effect (sometimes referred to as non-Darcy effect) which accounts for the additional pressure drop resulting from inter-pore-mixing appearing at high velocities (see, for instance, Plumb and Huenefeld [21]).

The appropriate boundary conditions suggested by the physics of the problem are

$$\begin{aligned} &u(x,0)=0,\ \nu(x,0)=0,\ T(x,0)=T_w=T_\infty+Ax^s \\ &u(x,\infty)=0,\ T(x,\infty)=T_\infty \end{aligned} \tag{4a-e}$$

where T_w is the wall temperature, A is a constant and s is a wall temperature parameter. It should be noted that when $s=0$, the constant wall temperature condition is recovered.

It is convenient to nondimensionalize the equations given before by using the following equations

$$\begin{aligned} &y=L\eta,\quad u=\frac{\nu x F'(\eta)}{L^2} \\ &\nu=\frac{-\nu(n+1)F(\eta)}{L},\quad T=T_\infty+(T_w-T_\infty)\theta(\eta) \end{aligned} \tag{5a-d}$$

where L is a characteristic length and a prime denotes ordinary differentiation with respect to η.

Upon substituting Eq. (5) into Eqs. (1) - (4), the following similarity equations and conditions result.

$$F''' + (n+1)FF'' - (1+\Gamma_x)(F')^2 - (M^2 + Da^{-1})F' + G_x\theta = 0 \tag{6}$$

$$\theta'' + Pr((n+1)F\theta' - sF'\theta) + \phi\theta = 0 \tag{7}$$

$$F'(0) = 0,\ F(0) = 0,\ \theta(0) = 1,\ F'(\infty) = 0,\ \theta(\infty) = 0 \tag{8a-e}$$

where

$$G_x = \frac{L^4 g\beta(T_w - T_\infty)\cos\alpha}{\nu^2 x},\ M^2 = \frac{\sigma_0 B_0^{\,2} L^2}{\rho\nu},\ Da = \frac{K}{L^2},\ \Gamma_x = Cx,\ Pr = \frac{\rho\nu c}{k_e},\ \phi = \frac{QL^2}{k_e} \tag{9a-f}$$

are the local Grashof's number, square of the Hartmann number, Darcy number, local inertia coefficient (Forchheimer number), Prandtl number, and the dimensionless heat generation parameter or heat sink/source parameter, respectively.

Of particular interest in this type of study are the skin-friction coefficient and the Nusselt number. These physical parameters are defined, respectively, as

$$C_f = \frac{C_f^{\,*}}{\rho\nu^2 x / L} = F''(0),\quad Nu = \frac{-h}{k_e(T_w - T_\infty)/L} = \theta'(0) \tag{10a, b}$$

where $C_f^{\,*}$ is the dimensional wall shear stress and h is the heat transfer coefficient.

Results and Discussion

The similarity equations given above are coupled, nonlinear, and exhibit no closed-form solution. Therefore, they must be solved numerically subject to the boundary conditions. The implicit finite-difference method with iteration similar to that discussed by Blottner [22] has proven to be successful for the solution of such equations and, for this reason, it will be employed herein.

The third-order differential equation is converted into a second-order differential equation by making variable changes. Then all second-order equations in η are discretized using three-point central difference quotients while the first-order equation is discretized using the trapezoidal rule. With this, the differential equations are converted into a set of algebraic equations which are solved with iteration (to deal with the nonlinearities of the governing equations) by the Thomas' algorithm (see, Blottner [22]). Most changes in the dependent variables are expected to occur in the vicinity of the wall where viscous effects dominate. Far away from the wall the fluid adjusts to the ambient conditions and changes in the dependent variables are expected to be small. For this reason, variable step sizes in η are employed in the present work. The initial step size $\Delta\eta_1$ was set to 0^{-3} and the growth factor was set to 1.03. These values are arrived at after many numerical experimentations which were performed to assess grid independence. A convergence criterion based on the relative difference between two successive iterations (set to 0^{-5} in the present work) was employed.

More details of the numerical solution and the procedure followed can be explained as follows:

Consider Eq. (6) governing the dimensionless function F. By defining

$$= F' \tag{11}$$

Eq. (6) may be written (before the central-difference formulas are used) as

$$\pi_1 V'' + \pi_2 V' + \pi_3 V + \pi_4 = 0 \tag{12}$$

where

$$\pi_1 = 1, \quad \pi_2 = (n+1)F$$
$$\pi_3 = -(M^2 + \mathrm{Da}^{-1}) - (1+\Gamma_x)V, \quad \pi_4 = G_x\theta \tag{13a-d}$$

Similarly, Eq. (7) can be written as

$$\pi_1 \theta'' + \pi_2 \theta' + \pi_3 \theta + \pi_4 = 0 \tag{14}$$

where

$$\pi_1 = 1, \quad \pi_2 = Pr(n+1)F$$
$$\pi_3 = \phi - Pr\, sV, \quad \pi_4 = 0 \tag{15a-d}$$

The boundary conditions for V and θ are

$$(0) = 0,\ V(\eta_{max}) = 0,\ \theta(0) = 1,\ \theta(\eta_{max}) = 0 \qquad (16a\text{-}d)$$

where infinity is replaced by η_{max} which is set to a maximum value of 10 in the present work.

The coefficients π_1, π_2, π_3, and π_4 in the inner iteration step of each of Eqs. (12) - (14) are evaluated using the solution from the previous iteration step. Eqs. (12) - (14) are then converted into tri-diagonal finite-difference algebraic equations which can be solved by the Thomas' algorithm.

Eq. (11) can be integrated by the trapezoidal rule to give

$$F_{n+1} = F_n + \frac{(V_{n+1} + V_n)\Delta\eta_n}{2} \qquad (17)$$

where n corresponds to the n^{th} point along the η direction and the boundary condition for F at $\eta = 0$ is

$$F(0) = 0 \qquad (18)$$

Figs. 2 - 3 present typical tangential (V) and normal (G) velocity, and temperature (θ) profiles for various values of the Hartmann number M, respectively. Physically speaking, the application of a transverse magnetic field normal to the flow direction results in a force opposite to the flow direction which tends to drag the flow, thus, slowing its motion. The effect of this force gets greater as the strength of the magnetic field increases. This is evident from the decreases in V and G as M increases observed in Fig. 1. However, in the absence of viscous and magnetic dissipations (which means lesser coupling between momentum and energy), the magnetic field has a negligible effect on the temperature profile. This is clearly shown in Fig. 2.

Figs. 4 - 5 illustrate the influence of the Darcy number Da on the velocity and temperature profiles, respectively. The presence of a porous medium in the flow presents resistance to flow, thus, slowing the flow and increasing the pressure drop across it. Therefore, as the inverse Darcy number ($1/Da$) increases, the resistance due to the porous medium increases and the velocity components decrease further as shown in Fig. 4. The value $Da = \infty$ corresponds to the case of no porous medium present. The effect of the porous medium is limited to the velocity profiles and has a negligible influence on the temperature profiles for the values of Da employed in Fig. 5.

Figs. 6 - 7 show the changes in the fluid tangential and normal velocities and temperature as the Prandtl number Pr is altered, respectively. It is observed from these figures that as Pr is increased, all of V, G, and θ decrease as is evident from Figs. 6 - 7.

Figs. 8 - 10 depict the variations in the skin-friction coefficient C_f and the Nusselt number Nu resulting from simultaneous changes in M, Da, and Pr. As mentioned before, increases in either of the Hartmann number M or the inverse Darcy number $(1/Da)$ or the Prandtl number Pr cause decreases in the tangential velocity and, in turn, its slope along the wedge surface. This results in decreases in the skin-friction coefficient C_f as either M or $1/Da$, or Pr increases. It should be noted that C_f approaches an asymptotic value for large values of M regardless of the values of Da and Pr. This means that the influence of M overrides that of Da and Pr as M becomes large. These behaviors are clearly shown in Figs. 8 - 9. Obviously, since changes in the values of M and Da, for small values of Pr have negligible influence on the temperature profiles, they will cause negligible changes in the temperature slope at the wedge surface. Thus, the Nusselt number which characterizes these changes will have negligible effect for small values of Pr as shown in Fig. 10. However, the reductions in θ as Pr is increased mentioned before cause θ' at the wedge surface to decrease resulting in a decrease in the values of Nu. It is noticed from Fig. 10 that as Pr increases the coupling between the flow and heat transfer increases through the Buoyancy effect and thus increases in the values of M at these conditions cause Nu to increase as clearly depicted in Fig. 10. It should be mentioned that in this figure when Da is altered, Pr was set to 0.71 and when Pr is varied, Da was set to 2.0.

Figs. 11 - 12 present profiles for V and G, and θ for different values of the heat generation coefficient ϕ, respectively. Increases in the values of ϕ have a tendency to increase the fluid tangential and normal velocities as well as its temperature. This is reflected in the increases in V, G, and θ shown in Figs. 11 - 12.

Figs. 13 - 14 illustrate the respective behavior of C_f and Nu as both M and ϕ are increased. The increases in both V and θ resulting from increasing ϕ cause the slopes V' and θ' at the wedge surface to increase. This has the direct effect of increasing C_f and Nu as is evident from Figs. 13 - 14, respectively.

It should be mentioned that it is observed from results not presented herein for brevity that increases in the Grashof's number G_x result in increases in V, G, and C_f, and slight decreases in θ and Nu. Furthermore, increasing the wall temperature exponent s causes slight reductions in all of V, G, θ, and C_f and slight increases in Nu.

As mentioned before, all the numerical results presented in Figs. 12 - 14 correspond to the case of a flow along a vertical wedge where $n = 0$. For $n = 1$ (case of a cone), very similar qualitative results are obtained. However, the quantitative values of the flow and heat transfer characteristics for the cone are lower than those of the wedge for the same parametric values. Table 1 summarizes some representative C_f and Nu results for the case of a cone ($n = 1$) in comparison with those reported by Vajravelu and Nayfeh [15]. It is seen that these results compare favourably. It can also be noted that as Γ_x increases, the resistance to the flow increases causing C_f to decrease and Nu to increase.

Conclusion

The problem of hydromagnetic free convection flow of an electrically-conducting and heat-generating fluid over a cone and a wedge supporting a uniform porous medium is considered. The governing partial differential equations are converted into ordinary differential equations by means for similarity variables for the case of non-uniform surface temperature. Numerical solutions of the resulting equations are obtained by the implicit finite-difference method. Graphical results illustrating special trends of the flow and heat transfer characteristics are presented and discussed. It was found that as either of the Hartmann number, or inverse Darcy number, or Prandtl number is increased, the skin-friction coefficient for the case of wedge or the cone decreases. The Nusselt number changes slightly as these parameters change and these changes become more pronounced as Pr and M get larger. It is also found that both the skin-friction coefficient and the Nusselt number increase as the heat generation source increases. Favourable comparisons with previously published theoretical work are performed. It should be mentioned that no comparisons with experimental data were made since these data are lacking at present.

References

1. E. M. Sparrow and R. D. Cess, Int. J. Heat Mass Transfer, **3**, 267 (1961).
2. N. Riley, J. Fluid Mech., **18**, 577 (1964).
3. H. K. Kuiken, J. Fluid Mech., **40**, 21 (1970).
4. H. S. Takhar, Indian J. Phys., **45**, 289 (1971).
5. G. Wilks, J. Appl. Math. Phys. (ZAMP), **27**, 621 (1976).
6. G. Wilks, J. Appl. Math. Phys. (ZAMP), **35**, 34 (1984).
7. H. S. Takhar and V. M. Soundalgekar, Appl. Sci. Res., **36**, 163 (1980).
8. K. Vajravelu and A. Rollins, Int. Comm. Heat Mass Transfer **19**, 701 (1992).

9. H. J. Merk and J. A. Prins, Appl. Sci. Res., **A4**, 11 and 195 (1953).

10. R. G. Hering and R. J. Grosh, Int. J. Heat Mass Transfer, **5**, 1059 (1962).

11. E. M. Sparrow and L. D. F. Guinle, Int. J. Heat Mass Transfer, **11**, 1403 (1968).

12. A. Nakayama, S. Ohsawa and H. Koyama, Letters Heat Mass Transfer, **9**, 445 (1982).

13. R. S. R. Gorla and R. A. Stratman, Int. Comm. Heat Mass Transfer **13**, 403 (1986).

14. T. Watanabe and I. Pop, Int. Comm. Heat Mass Transfer, **20**, 871 (1993).

15. K. Vajravelu and J. Nayfeh, Int. Comm. Heat Mass Transfer, **19**, 701 (1992).

16. K. Vafai and C. L. Tien, Int. J. Heat Mass Transfer, **25**, 1183-1190 (1982).

17. J. T. Hong, Y. Yamada and C. L. Tien, ASME J. Heat Transfer, **109**, 356-362 (1987).

18. D. Moalem, Int. J. Heat Mass Transfer, **19**, 529 (1976).

19. L. Topper, J. Ame. Inst. Chem. Engrs., **1**, 463 (1955).

20. F. P. Foraboschi and I. D. Federico, Int. J. Heat Mass Transfer, **7**, 315 (1964).

21. O. A. Plumb and J. C. Huenefeld, Int. J. Heat Mass Transfer, **24**, 765 (1981).

22. F. G. Blottner, AIAA J., **8**, 193 (1970).

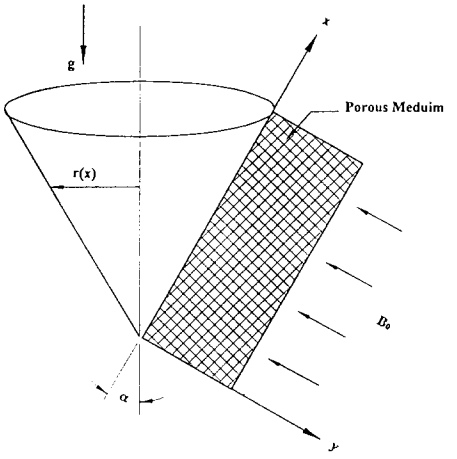

FIG. 1
Flow Model and Coordinate System

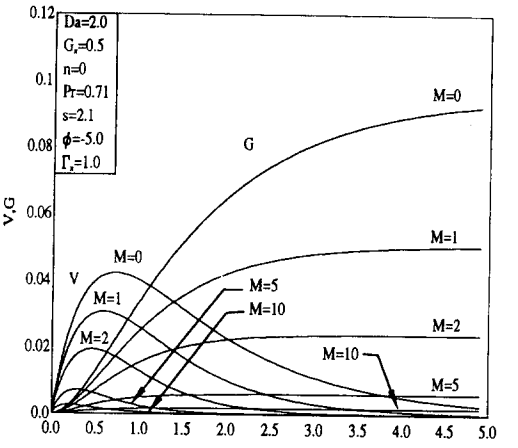

FIG. 2
Effect of M on the Tangential and Normal Velocity Profiles

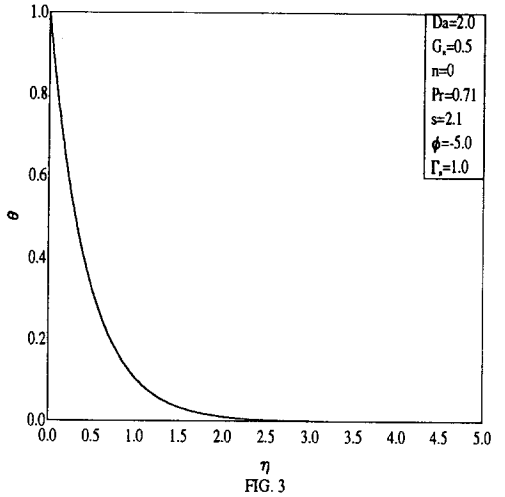

FIG. 3
Effect of M on the Temperature Profiles

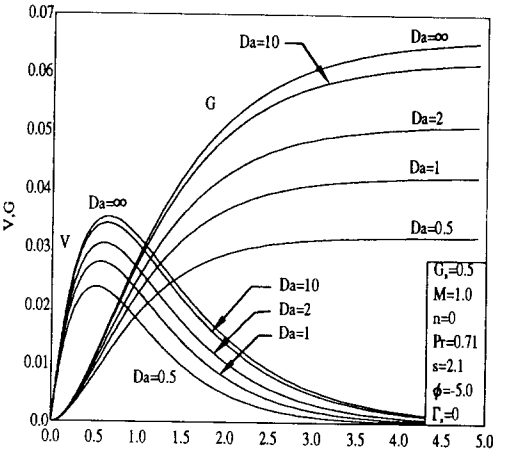

FIG. 4
Effect of Da on the Tangential and Normal Velocity Profiles

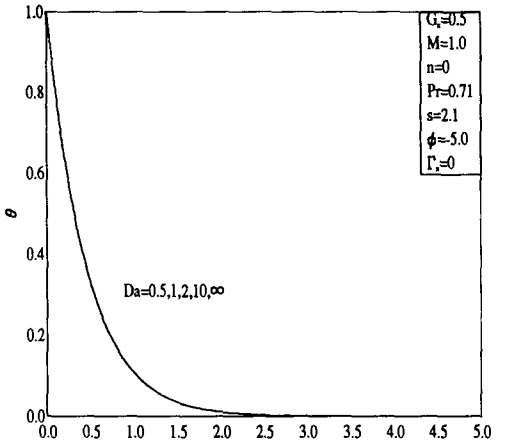

FIG. 5
Effect of Da on the Temperature Profiles

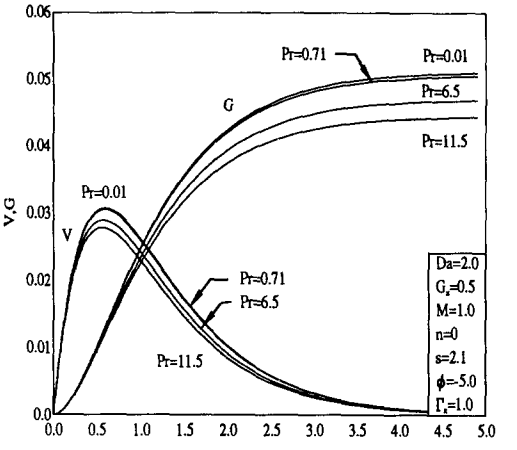

FIG. 6
Effect of Pr on the Tangential and Normal Velocity Profiles

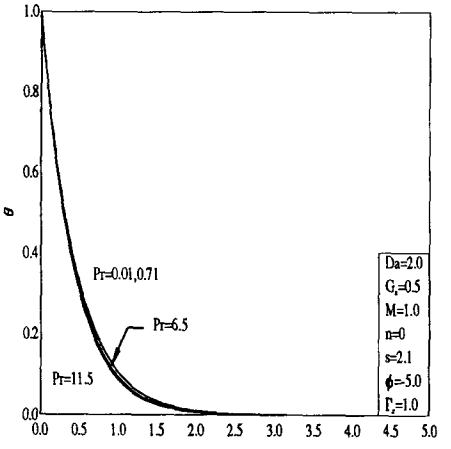

FIG. 7
Effect of Pr on the Temperature Profiles

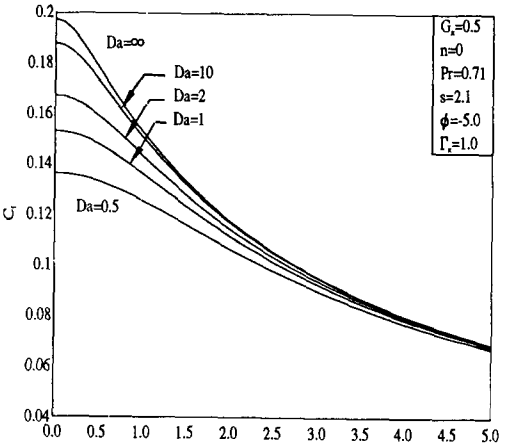

FIG. 8
Effects of M and Da on the Skin-Friction Coefficient

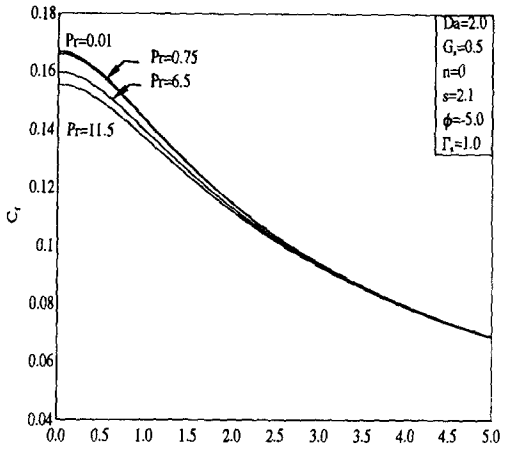

FIG. 9
Effects of M and Pr on the Skin-Friction Coefficient

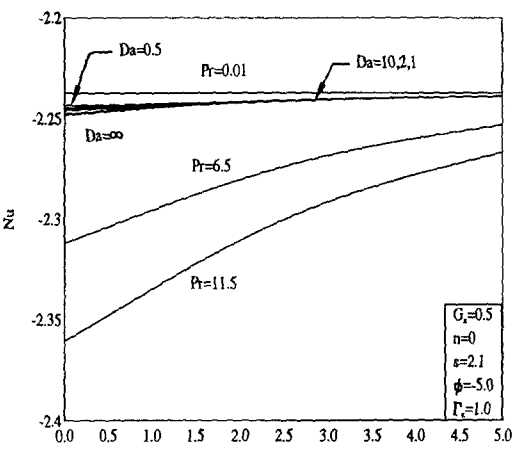

FIG. 10
Effects of M, Da, and Pr on the Nusselt Number

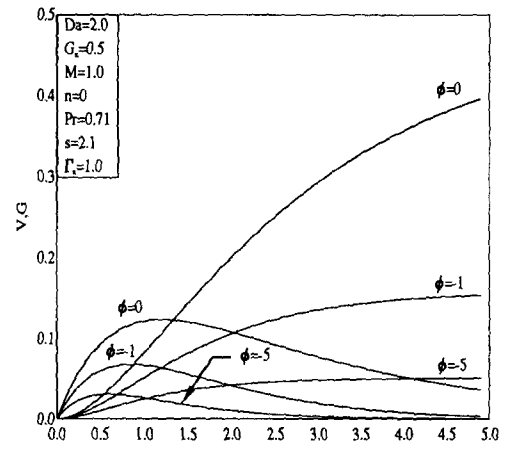

FIG. 11
Effect of ϕ on the Tangential and Normal Velocity Profiles

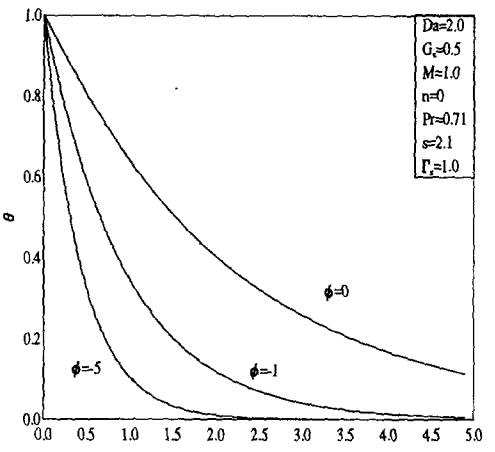

FIG. 12
Effect of ϕ on the Temperature Profiles

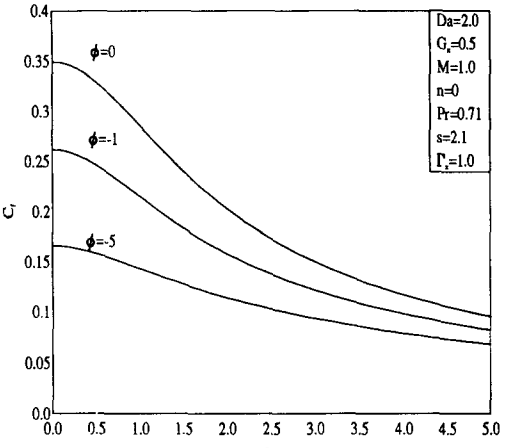

FIG. 13
Effects of M and ϕ on the Skin-Friction Coefficient

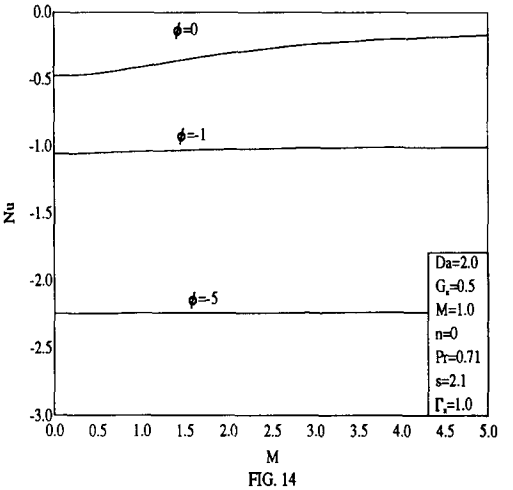

FIG. 14
Effects of M and ϕ on the Nusselt Number

TABLE 1
Comparison of present C_f and Nu values with those reported by [15] for a cone ($n = 1$)

ϕ	Pr	G_x	M^2	s	Da	Γ_x	C_f [15]	Nu [15]	C_f present	Nu present
-5	0.3	-0.5	1	-2.1	0	0	-0.155592	-2.237475	-0.155592	-2.238739
-5	0.3	-0.5	1	2.1	0	0	-0.156001	-2.232780	-0.155995	-2.234070
-5	0.3	-0.5	3	2.1	0	0	-0.126400	-2.233732	-0.126403	-2.234680
-5	0.3	0.5	3	2.1	0	0	0.125618	-2.238864	0.125612	-2.240234
-1	1.0	-0.5	1	1	1	1	--	--	-0.217901	-0.955566
-1	1.0	-0.5	1	1	1	3	--	--	-0.222947	-0.953552

Received December 27, 1995